1

MoS$_2$ quantum dots for on-line fluorescence determination of the food additive

allura red in beverage

Alicia Coloma[a], María del Pozo[a]*, Rut Martínez-Moro[a], Elias Blanco[a], Pedro Atienzar[b],

Lorenzo Sánchez[c], María Dolores Petit-Domínguez[a], Elena Casero[a], Carmen Quintana[a]

[a]*Departamento de Química Analítica y Análisis Instrumental, Universidad Autónoma de Madrid, Cantoblanco, 28049 Madrid, Spain.*

[b]*Instituto Universitario de Tecnología Química CSIC-UPV, Departamento de Química, Universidad Politécnica de Valencia, 46022 Valencia, Spain.*

[c] *Departamento de Medio Ambiente. Geología Ambiental Aplicada. CIEMAT. Avda. Complutense, 40 Edif. 85, 28040 Madrid. Spain*

*maria.delpozo@uam.es; Phone: +34 914975916; Fax: +34914974931

17   **Abstract**

18   This work presents an on-line fluorescence method for the allura red (AR)

19   determination. The method is based on the fluorescence quenching of dots of MoS_2

20   because of their interaction with the non-fluorescence dye. MoS_2-dots were synthetized

21   and characterized by spectroscopic techniques and High Resolution Transmission

22   Electronic Microscopy (HR-TEM). The simultaneous injection of the nanomaterial and

23   the dye in a flow injection analysis system allows the determination of allura red at 1.7

24    $\times 10^{-6}$ M concentration level with a very good accuracy and precision (Er minor than

25   10% and RSD lower than 8%) and a sampling frequency of 180 samples per hour.

26   Moreover, the interaction fluorophore-quencher results a dynamic inhibition

27   mechanism. The proposed methodology was applied to the AR analysis in soft

28   beverages and powders for gelatine preparation. Colourant concentrations of 63 ± 2 mg/L

29   (n=3) and 0.30 ± 0.01 mg/g (n=3) were found, respectively. These results were validated

30   by high performance liquid chromatography technique.

31   **Keywords:** Molybdenum disulfide, dots, fluorescence inhibition, allura red, food

32   additive, flow injection analysis.

33

34

35

1. Introduction

Transition metal dichalcogenide (TMDs) nanomaterials are currently attracting the interest of the scientific community because of their promising utilities. TMDs present chemical formula of MX_2, where X belongs to a chalcogenide group, M is a transition metal and both make layers where the metal is located between two layers of chalcogenides, as a sandwich. The adjacent MX_2 layers are bonded through Van der Waals forces, so this weak interaction allows these nanomaterials to be easily exfoliated to thin layers. Therefore, several TMDs nano-morphologies have been reported that can be categorized in different dimensionalities as sheets (2D), nanoribbons and nanotubes (1D) or dots and nanoparticles (0D) (Li et al., 2016). Although many combinations of M and X have been disclosed, molybdenum disulfide and tungsten disulfide are the most frequently employed TMDs. (Bouša et al., 2018; Coleman et al., 2011; S. Xu, Li, & Wu, 2015; X. Zhang et al., 2015)

TMDs nanostructures are produced following bottom-up or top-down approaches.(Sun et al., 2017) Bottom-up syntheses are based on the reaction of metal transition salts with chalcogenide ions, while the stacked structure of bulk TMDs makes them feasible to top-down methods. The most common top-down approach is the ultrasonic-assisted liquid exfoliation in appropriated solvents as N-methyl-pyrrolidone (NMP), dimethylformamide (DMF) or ethanol/water. The advantages of this strategy are such as cheap, easy, scalable and effective, efficiency that is boosted for solvents that minimize the exfoliation enthalpy as NMP. (Huang, Zeng, & Zhang, 2013; Lesnyak, Gaponik, & Eychmu, 2013)

Nanosheets and dots made of TMDs have exhibited their usefulness in the analytical discipline. (Sinha et al., 2018; Vilian et al., 2019) The intrinsic TMDs-dots photoluminescence has encouraged fluorescence methodologies while 2D-TMDs are

more likely to be employed for the development of electrochemical sensors (Vilian et al., 2019). The former approach is based on the ability of some analytes to absorb the photons that dots emit so the output is the dots signal quenching. (Cao et al., 2018; Guo, Wang, Wu, Ni, & Kokot, 2015; X. Liu et al., 2018; Yong Wang & Ni, 2014; Zhao et al., 2017) From this point of view, colourants could be good candidates as analytes in quenching-based methodologies due to their inherent absorption properties.

Colourants are additives in a wide variety of foodstuff giving colour and improving their organoleptic properties. These additives can be classified as natural, semisynthetic and synthetic. Chlorophylls, carotenoids or anthocyanins (natural colourants) are harmless but scarcely resistant to temperature changes, pH or solar radiation (Damodaran, Parkin, & Fennema, 2007). For this reason, synthetic colourants are widely used. This kind of additives are easily synthesized, stables and cheap (Bişgin, 2019). In addition, the sulphonic groups that are present in their chemical structure confer them high solubility in water. The main disadvantage of synthetic colourants is that they usually present azo groups together with aromatic rings in their structures, so they are potentially carcinogens and allergens and can cause hyperactivity in children (Carocho, Barreiro, Morales, & Ferreira, 2014; Ivani de Andrade et al., 2014). Some of these azo-colourants are tartrazine (E-102), sunset yellow (E-110), ponceau 4R (E-124) and allura red (E-129). Its analytical determination has been accomplished by several techniques but especially by high performance liquid chromatography with UV-Vis detector (HPLC-UV-Vis), UV-Vis spectrometry and electrochemical techniques (Bişgin, 2019; Ivani de Andrade et al., 2014; Magerusan et al., 2018). Although colourants are not usually fluorescent, indirect methods based on the interaction with nanomaterials have demonstrated their success (H. Xu, Yang, Li, Zhao, & Liao, 2015).

85 Flow injection analysis (FIA) is appealing when fast, simple and efficient method is

86 required in routinely performed analysis. These procedures allow automation and

87 miniaturization of analytical methodologies so they have been recognized as very useful

88 in areas such as environmental, industrial and/or clinical analysis. The simple use of its

89 instrumentation makes FIA methods attractive to researchers in the development of

90 analytical methodologies with on-line detection. In addition, a great variety of detectors

91 have been successfully coupled with FIA systems (Trojanowicz & Kołacińska, 2016).

92 In this work, MoS_2-dots were synthetized and evaluated against the colourant Allura

93 red, employed as food additive. As a result, an on-line FIA method for the

94 determination of this non-fluorescent synthetic dye is developed. The method is based

95 on the fluorescence inhibition of MoS_2-dots due to the interaction with the analyte. The

96 Allura red concentration is monitored thanks to the simultaneous injection of the

97 nanomaterial and the colourant in the flow system. The development of a flow method

98 based on this interaction for the fast and sensitive analysis of non-fluorescent analytes

99 with high sample frequency, results a promising strategy that can be extended to

100 different non-optically active compounds of interest.

101 **2. Materials and Methods**

102 2.1 Reagents

103 Molybdenum disulfide powder (90 nm, 99%), quinoline yellow, sunset yellow,

104 ponceau 4R, carmoisine, amaranth, sodium citrate, sodium chloride, quinine, glucose,

105 fructose and allura red were obtained from Sigma Aldrich (www.sigmaaldrich.com). N-

106 methylpirrolidone (NMP), orthophosphoric acid, methanol for HPLC, ammonium

107 acetate, acetone and sodium hidroxide were purchased from Scharlab, Spain

108 (www.scharlab.com). Nitric acid for measurements by ICP-MS was tri-distilled

commercial concentrate from Scharlab. Water was purified with a Millipore Milli-Q-System. All solutions were prepared just before use. Inorganic Ventures (Christiansburg, USA) supplied the certified reference molybdenum (995±6 μg/mL) standard for ICP-MS analysis.

2.2 Apparatus

For the MoS_2-dots synthesis, an ultrasound bath (Transonic 570/H Elma) was used. Both, a spectrophotometer Shimadzu UV-1800 and a spectrofluorometer Hitachi F-7000 were employed for optical measurements. A pH meter Methrom C831 (Herisau Switzerland) was used for buffers preparations. The Flow Injection Analysis system employed consisted of i) a peristaltic pump (Heidolph 5201), ii) a 12 ports injection valve (Teknokroma Analítica S.A) equipped with two loops that allows the synchronized injection of nanomaterial and the analyte, converging both at the beginning of iii) the reactor tube producing a homogeneous solution of both reagents and iv) the spectrofluorometric detector operating at fixed excitation and emission wavelengths. A High Performance High Resolution (Element 2) (Thermo Scientific) was employed for Inductively Coupled Plasma - Mass Spectrometry (ICP-MS) measurements. Before the ICP-MS measurements, an acid purification system from Savillex (Eden Prairie, USA) was employed for nitric acid tri-distillation.

High Performance Liquid Chromatography (HPLC) measurements were performed with a Jasco Analytica PU-1580 high pressure pumping system, equipped with an injector Rheodyne Model 7125, a 20 μL loop and a Kromasil C18 column (150 x 4.6 mm; 5 μm; Scharlau). A Perkin Elmer 785A UV/VIS was employed as detector of the chromatographic system.

132 High Resolution Transmission electron microscopy (HR-TEM) images were acquired

133 with a transmission electron microscope (JEOL JEM 2100F, Tokyo, Japan) under an

134 accelerating voltage of 200 kV. Samples were prepared by applying one drop of the as-

135 synthesised nanodots in NMP onto a carbon-coated copper TEM grid, and allowing it to

136 dry at room temperature. TEM images were analyzed by using Gatan Digital

137 Micrographs software.

138 ### 2.3 Procedures

139 #### 2.3.1. *MoS$_2$-dots synthesis*

140 MoS$_2$-dots were synthesized following a previously reported method (S. Xu, Li, & Wu,

141 2015) with slight modifications: around 100.00 ± 0.01 mg of the bulk MoS$_2$ reagent was

142 added to 10.0 mL of NMP and the suspension was exfoliated in an ultrasound bath

143 during 3 h and then heated at 140 °C under stirring during 6 h. After leaving to rest

144 overnight, the mixture was centrifuged at 4000 rpm for 45 minutes. MoS$_2$-dots were

145 separated in the supernatant and kept at 4 °C until use. From the ICP-MS analysis of the

146 as-prepared nanomaterials, it was found a synthesis yield of 2.02%.

147 #### 2.3.2. *Spectroscopic measurements*

148 Absorbance spectra were acquired between 250 and 800 nm with a 1 cm quartz cuvette.

149 For spectrofluorometric measurements, an excitation wavelength (λ_{ex}) of 370 nm was

150 employed with a slit of 5.0 nm and the fluorescence was recorded from 380 to 600 nm

151 with 1 cm path length when static measurements were performed.

152 The MoS$_2$-dots concentration was quantified by ICP-MS. To this end, after the solvent

153 evaporation, the MoS$_2$-dots were dissolved in a 1:1 (v/v) HNO$_3$:HCl mixture, as

154 previously described in the literature (W. Zhang et al., 2015). After an adequate

155 dilution, the samples were subjected to ICP-MS determination. The Mo quantification

156 was performed at low resolution (LR) at m / ΔM = 300. The tune parameters employed

157 were: plasma power = 1258 Watt, pump speed=15 rpm, cool gas = 16 L/min, auxiliary

158 gas =1.3 L/min, sample gas = 1.2 L/min, extraction voltage = -2000 V, SEM = 1900 V.

159 Mass spectrometric data were acquired in EScan mode at the following conditions:

160 segment duration = 0.15 s, settling time = 0.001 s, sample time = 0.015 s, samples per

161 peak = 50, acquired points = 10, detection mode = analogical + counting, integration

162 window = 20%. The isotope ^{95}Mo was monitored, in a mass range of 94.874 - 94.937 u

163 and with the same mass window of 20%. Sample introduction was performed with a

164 peltier cooled inlet system with quartz cyclonic spray chamber (ESI: Elemental

165 Scientific Instruments, Omaha EEUU).

166 FIA measurements were carried out with fluorescence detection at λ_{exc} = 370 nm and an

167 emission wavelength (λ_{em}) of 475 nm. H_3PO_4/NaH_2PO_4 0.1M buffer pH =2 was

168 employed as carrier solution pumped at a constant flow rate of 3 mL/min. A volume of

169 100 μL of MoS_2-dots (150 fold diluted in water) and 100 μL of analyte were

170 synchronously injected in the flow system and the successive reaction was produced in

171 a 40 cm reactor with an internal diameter of 0.5 mm.

172 HPLC-UV measurements were performed following a previously reported procedure

173 (Yu & Fan, 2016) with a flow rate of 0.7 mL/min.

174 *2.3.3. Sample preparation*

175 Two commercially samples were acquired in a local market, a carbonated drink and a

176 powder for gelatine preparation. The soft drink of strawberry flavour was degassed

177 under stirring and, after 10 times dilution with carrier solution, was injected in the FIA

178 system. For HPLC-UV analysis, the carbonate drink samples were degassed as

179 described above and diluted (1:10) with Methanol/ammonium acetate 0.02 M (35/65,

8

180 v/v) employed as mobile phase. Next, the diluted samples were filtered through a 0.45

181 μm pore size nylon filter before injection in the chromatographic system.

182 An accurate amount of gelatine sample of around 3.00000 ± 0.00001 g was crushed

183 with a mortar. The sample was successively extracted first with methanol and then with

184 acetone by tip sonication according to a published procedure (Shen, Zhang,

185 Prinyawiwatkul, & Xu, 2014). After centrifugation at 4000 rpm for 5 minutes, the

186 extracts were mixed up and evaporated under nitrogen stream until nearly dryness. The

187 residue was reconstituted in methanol and filled up to 5.00 mL. Before to be injected in

188 the FIA system, 150 μL of the extract were diluted to 1.00 mL in the carrier solution.

189 For HPLC analysis, 15 μL of the sample extract were diluted with mobile phase to 5.00

190 mL before filtration and injection.

191

192 **3. Results and discussion**

193 3.1 Nanomaterials characterization

194 *3.1.1. High-Resolution Transmission Electron Microscopy experiments*

195 The synthesized dots of MoS_2 were characterized by HR-TEM to obtain information

196 related to its particle size and crystallinity. Figure 1A shows an example of the HR-

197 TEM images obtained where individual and very small nanoparticles of around 5 nm or

198 minor, are observed. Moreover, in the marked zone of the image, the lattice fringes

199 revealing the nanoparticles crystallinity can be clearly observed, also Fast Fourier

200 Transform (FFT) analysis support this observation. From the data of N = 90

201 nanoparticles, a mean diameter of (3.4 ± 0.9) nm was calculated. The electron

202 diffraction (SAED) pattern of the inset in Figure 1A reveals the hexagonal lattice

203 structure with a lattice parameter of 0.27 nm (calculated from inverse FFT image after

204 selecting the diffraction spots) and similar with the direct measurement of profile plot

205 (Figure 1B and 1C), consistent with the (100) diffraction planes of MoS_2 (Ha, Han,

206 Choi, Park, & Seo, 2014; Q. Liu, Hu, & Wang, 2016; Yichao Wang et al., 2013).

207 FIGURE 1 HERE.

208

209   *3.1.2. Spectroscopic characterization*

210 First, the MoS_2-dots concentration was evaluated by the ICP-MS procedure described

211 above. Figure S1 depicts the calibration graphs corresponding to the Mo determination.

212 From this analysis, the concentration MoS_2-dots was 0.202 mg/mL.

213 Next, the MoS_2-dots synthesized in NMP were subjected to spectroscopic

214 characterization after a 1:100 dilution in water. The MoS_2-dots UV-Vis spectrum

215 (Figure S2A) displays two absorption bands centred at 270 and 340 nm. These two

216 bands are the maxima characteristic of TMDs-dots and are ascribed to the electronic

217 transitions of π to π^* and n to π^*, respectively (X. Liu et al., 2018). Notice that no

218 features were recorded at longer wavelengths. Unlike TMDs-dots, TMDs-nanosheets

219 show up to four absorption bands in the 390-680 nm domains so the effective

220 transformation of nanolayers into dots can be concluded (X. Liu et al., 2018; Wilcoxon,

221 Newcomer, & Samara, 1997; H. Xu et al., 2015; S. Xu et al., 2015a). Moreover, as

222 stated in the introduction section, TMDs-dots have inherent photoluminescence (Štengl

223 & Henych, 2013). For this reason, it was recorded the emission spectra at different

224 excitation wavelengths around both UV-Vis maximums. The spectra in Figure S2B

225 confirm that: i) a luminescent nanomaterial was synthetized as expected; ii) irrespective

226 of the excitation wavelength (λ_{exc}) used, MoS_2-dots present an emission band with a

227   maximum at 458 nm (λ_{em}); iii) the fluorescence intensity depends on λ_{exc}, recording the

228   highest intensities when exciting at λ_{exc} 270 and 370 nm.

229   The influence of the pH of the solution on the MoS_2-dots fluorescence was tested by

230   varying the pH solution in which the dots suspension was diluted. Figure S3 depicts the

231   results corresponding to MoS_2-dots excitation at 370 nm. As observed, the fluorescence

232   intensity decreases as pH increases, recording the maximum fluorescence value at acidic

233   media. Moreover, the fluorescence signal is not affected by the presence of salts in

234   solution as can be concluded by comparing the spectra recorded in un-buffered water

235   and neutral pH phosphate buffer. It should be noted the large decrease in the signal

236   showed at alkaline conditions. This pH dependence was also observed when 270 nm

237   λ_{exc} was used (data not shown). As the highest intensity signal is obtained with 0.1 M

238   H_3PO_4/NaH_2PO_4 pH 2, this pH was selected as the measurement medium for the rest of

239   experiments.

240   In this pH 2 medium, we calculated the relative fluorescence quantum yield of the

241   MoS_2-dots, employing quinine as standard (Φ tabulated $\lambda_{exc\ 275\ nm} = 0.577$) and

242   according to equation 1 below:

$$\Phi_x = \Phi_s \frac{A_s}{A_x} \cdot \frac{F_x}{F_s} \cdot \left(\frac{n_x}{n_s}\right)^2$$

243   **Equation 1**. Φ = fluorescence quantum yield, A = absorbance at λ_{exc}, F = emission

244   curve area, n = solvent refraction index. Subscripts *s* and *x* correspond to the standard

245   and the analyte respectively.

246   From the results, a value of 8.6% was obtained which is similar or better that other

247   values previously reported in the literature for MoS_2-dots and carbon dots (Cao et al.,

248   2018; Yong Wang & Ni, 2014; Z. Wang & Dai, 2015).

250   3.2 MoS$_2$-dots interaction with Allura red. Static conditions.

251   The absorbance spectrum of a 2.0×10^{-5} M AR solution shows two absorption bands

252   between 300 and 600 nm (Figure 2A, curve a). However, it is important to note that no

253   fluorescence is registered for this dye neither when exciting at its maximum absorption

254   wavelength (500 nm) or exciting at the MoS$_2$-dots excitation wavelength (270 and 370

255   nm) (data not shown). In addition, Figure 2A includes the fluorescence spectra of MoS$_2$-

256   dots (dotted lines). As can be seen, these emission spectra overlap in a great extent with

257   the absorption spectrum of the colourant. This result led us to expect an interaction

258   between the nanomaterial and the AR based on the energy/photon transfer of MoS$_2$-dots

259   emission to the colourant.

260   FIGURE 2 HERE

261   To verify the interaction of the nanomaterial with AR, the fluorescence spectra of a

262   solution containing a mixture of both, MoS$_2$-dots and AR, were registered either at $\lambda_{exc}=$

263   270 nm or $\lambda_{exc} = 370$ nm. Figure 2B shows the fluorescence response of the dots and the

264   dots in presence of 2.0×10^{-5} M of AR at $\lambda_{exc} = 370$ nm. As observed, the nanomaterial

265   fluorescence is greatly quenched in presence of AR probably because of the analyte

266   absorbs the nanomaterial emission leading to a fluorescence reduction in a dynamic

267   mechanism as will be latter discussed. The same behaviour is observed when excitation

268   is performed at 270 nm (data not shown). We selected 370 nm as excitation wavelength

269   since better selectivity is expected than working at lower excitation conditions.

270   Once the nanomaterial-AR interaction was experimentally confirmed, a deeper study of

271   this interaction was carried out. The Stern-Volmer constant (K_{sv}) determines the degree

272   of interaction fluorophore - quencher (Lakowicz, 2006) and it is calculated from the

273   same name equation:

$$\frac{If_0}{If} = 1 + K_{sv}[Q]$$

274   **Equation 2.** Stern-Volmer equation.

275   In this equation, If_0 and If correspond to the MoS_2-dots emission in absence and in

276   presence of a concentration of colourant, $[Q]$. The meaning of the calculated constant is

277   that the higher the K_{sv} value, the stronger the interaction. For K_{sv} determination, the

278   MoS_2-dots spectrum was registered in presence of increasing concentrations of AR.

279   Figure 3 shows the obtained results of If_0/If versus AR concentration. The monitoring of

280   the dots emission was performed at λ_{em} of 475 nm where the quenching due to the

281   interaction with AR is more remarkably produced (see Figure 2B). This experiment was

282   performed at different temperature values.

283   FIGURE 3 HERE

284

285   As shown in Figure 3, linear relations between If_0/If and AR concentration are obtained

286   in all experiments. From the corresponding slopes, the K_{sv} values can be calculated (see

287   the legend Figure 3). Data shows a slight increase in K_{sv} with the temperature. This

288   increase would imply a dynamic inhibition mechanism in which diffusion could control

289   the interaction. This diffusion is favoured by increasing the temperature, making greater

290   the constant value (X. Liu et al., 2018).

291   Finally, the influence of the concentration of MoS_2-dots was studied to obtain the best

292   analytical response in terms of sensitivity. To this aim, several nanomaterial dilutions

293   (1:50-1:200) in 0.1 M H_3PO_4/NaH_2PO_4 pH 2 were prepared and assayed against two

294   analyte concentration levels, $[AR] = 1.25 \times 10^{-6}$ M and $[AR] = 2.00 \times 10^{-5}$ M (data not

295   shown). From the results, the best accomplishment was obtained for a 150-fold dilution.

296   Therefore, this condition was selected for the development of the FIA analytical method

297   towards the on-line AR determination.

298   <u>3.3 MoS_2-dots interaction with AR in flow conditions. FIA experiments.</u>

299   FIA measurements were carried out with fluorescence detection at λ_{exc} = 370 nm and an

300   emission wavelength (λ_{em}) of 475 nm. Figure S4 shows that the synchronized injection

301   of MoS_2-dots and AR produces a decrease in the height peak confirming the interaction

302   MoS_2-dots-AR in the carrier flow towards the fluorescence detection system. This

303   simple experiment allows us to conclude that the quenching effect can be monitored

304   also under flow conditions. Therefore, the optimization of the experimental variables

305   affecting to the FIA system was following made.

306

307   *3.3.1. FIA optimization: hydrodynamic and geometric parameters.*

308   The hydrodynamic and geometric parameters involved in the FIA response were

309   optimized in order to obtain the highest fluorescence quenching (% $If_0 = \frac{If}{If0} \cdot 100$) as

310   well as the highest sample frequency. Caudal (Q), reactor length (L), reactor internal

311   diameter (Di) and injection volume (Vinj) were optimized. First, the influence of the

312   carrier flow rate was evaluated in the 1 to 4 mL/min range. The results did not show a

313   noticeable influence in the % If_0 but the sample frequency increases while increasing the

314   caudal, because of the decrease of the peak width (Figure S5). This effect is produced

315   up to a flow rate value of 3 mL/min, when the signal is stabilized. Therefore, this flow

316   rate was considered as optimal for the rest of experiments.

317 Six reactors were used to optimize length (L = 40, 70 and 100 cm) and internal diameter

318 (Di = 0.5 and 0.8 mm). As seen in Figure S6, the thinnest internal diameter reactor

319 showed better %If$_0$ regardless of the length. For each Di value, a shortened reactor

320 showed a slightly better %If$_0$. In base of these results, a reactor with Di = 0.5 mm and L

321 = 40 cm was selected for the analytical determination.

322 Sample loops were simultaneously varied between 50 and 200 μL volume keeping the

323 same volume for the analyte and the MoS$_2$-dots. As in previous experiments, %If$_0$ was

324 scarcely affected. However, it was found that the higher the loop volume, the wider the

325 FIA signal peaks so poorer sampling frequencies were registered. From the results

326 (Figure S7), 100 μL volume was fixed for further assays. Altogether, the optimal

327 parameters summarized in Table S1 allow the analysis of 180 samples/h in conjunction

328 with a good fluorescence inhibition.

329   *3.3.2. Influence of AR concentration in the analytical response. Analytical data*

330 Once all the variables affecting the FIA system were optimized, the quenching in the

331 fluorescence intensity of MoS$_2$-dots with increasing AR concentrations was studied.

332 Figure 4 shows that a linear decrease of the initial signal was obtained in the AR

333 concentrations range of 5.00×10^{-6} M to 4.00×10^{-5} M according to the equation: %If$_0$ =

334 $-1.2 (\pm 0.3) \times 10^{6}$ [AR] (M) + 99.0 ($\pm$ 0.6); r=0.995.

335 FIGURE 4 HERE

336 Detection limit (LOD) and determination limit (LOQ) for the analytical method were

337 calculated from the standard deviation (σ) of 10 injections of MoS$_2$-dots in the FIA

338 system and the slope of the corresponding linear range of the calibration curve. The

339 obtained values were 1.7×10^{-6} M and 5.6×10^{-6} M for LOD (3σ/slope) and LOQ

340 (10σ/slope), respectively. These results are comparable with those reported in the

15

341   literature for the AR determination with different analytical methodologies (see Table

342   S2) (Al Shamari et al., 2020; Deroco, Medeiros, Rocha-filho, & Fatibello-filho, 2018;

343   Mazdeh et al., 2016; Rodriguez, Ibarra, Miranda, Barrado, & Santos, 2016; Silva,

344   Garcia, Lima, & Barrado, 2007; Tang et al., 2018; Vidal, Garcia-Arrona, Bordagaray,

345   Ostra, & Albizu, 2018). Compared with the analytical methods summarized in Table S2,

346   the proposed method presents several advantages such as allowing a fast analysis with a

347   high sample frequency and the possibility of an on-line analysis automation.

348   Table 1 summarizes the results obtained to evaluate the accuracy and the precision in

349   terms of the relative error (Er %) and the relative standard deviation (RSD %). The

350   precision was assessed in both, repeatability and reproducibility for five concentrations

351   levels. As seen, the developed method presents Er (%) values lower than 10% and

352   excellent results in terms of repeatability and reproducibility with RSD (%) values

353   lower than 1.3% and 8%, respectively.

354

355   **Table 1.** Er (%) and RSD (%) for the developed method at different AR concentrations.

[AR] (M)	Er (%)	RSD (%) $_{(n = 3)}$ repeatibility	RSD (%) $_{(n = 3)}$ reproducibility
1.25×10^{-5}	4.0	0.6	3
1.50×10^{-5}	6.7	0.7	4
2.00×10^{-5}	10	0.3	6
3.00×10^{-5}	3.3	1.2	8
4.00×10^{-5}	5.5	1.3	7

356

357   *3.3.3. Interference study*

358   The selectivity of the method was evaluated by the change that it is produced in the

359   fluorescence signal of a mixture of MoS$_2$-dots with 2.00×10^{-5} M of AR in presence of

360   increasing amounts of different compounds that can be present in a sample together

361 with the analyte. It was considered that interference is produced at a concentration level

362 that led to a change in the initial analytical signal bigger than the relative error of the

363 method (10%). Sodium citrate, sodium chloride, glucose and fructose were selected

364 because they are usually found in carbonated drinks. Both salts can be present in high

365 concentration respect to AR, even to 200-fold, without produce interference.

366 Concerning glucose and fructose, the obtained results show that the maximum

367 concentrations allowed without producing interference are 0.37 M and 0.055 M,

368 respectively. These results show the possibility to determine AR in presence of high

369 concentration of sugar. The rest of compounds assayed were other colourants that can

370 also appear with the analyte in some samples. Amaranth, quinoline yellow, ponceau 4R,

371 carmoisine and sunset yellow interfere for a concentration higher than 2.80×10^{-5} M,

372 2.03×10^{-5} M, 8.03×10^{-6} M, 1.50×10^{-5} M and 2.00×10^{-5} M, respectively. These

373 results show that it is possible to determine AR in presence of other colourants.

374

375 *3.3.4. Application to AR determination in real samples.*

376 The feasibility of the method was tested towards the AR determination in real samples

377 of a commercial carbonated drink of strawberry flavour and a powder to prepare

378 gelatine. The procedures for each sample preparation were previously detailed in the

379 experimental section. In the case of the carbonated drink, only a degas pre-treatment of

380 the beverage was needed. The determination was carried out by the injection in the FIA

381 system of non-spiked samples and samples spiked with increasing AR concentrations.

382 The FIAgrams in Figure 5 show the decrease produced in the MoS_2-dots fluorescence

383 intensity when the non-spiked sample was injected. This fact allows us to conclude the

384 presence of AR in the selected sample, as it was described in the available information

385 of the drink. As expected, the fluorescence quenching linearly increases with increasing

386   amounts of AR added according to the equation: $\%If_0 = (-1.2 \pm 0.6) \times 10^6$ [AR] (M) +

387   (82.5 ± 0.7); r = 0.994. As observed, the slope obtained with the standard addition

388   method is the same than that gotten with the external calibration procedure described

389   before. This fact suggests that no matrix interference was produced. Therefore, the

390   external calibration was employed to determine the AR concentration in the sample

391   obtaining a value of 63 ± 2 mg/L (n= 3) of AR in the beverage. Due to the legal limit

392   established by the Council of the European Union of AR in this kind of samples is 100

393   mg/L, this sample is appropriate for human consumption (Union, 1994). The recovery

394   of the method was evaluated from the analysis of an initially spiked sample at $2.00 \times 10^{-}$

395   ^{5} M AR concentration. A recovery of 105% with a RSD of 3.8% as average of three

396   independent analyses was calculated.

397   For the AR determination in gelatine samples, aliquots of 150 µL of non-spiked and

398   spiked with increasing AR amounts sample extracts (obtained as described in section

399   2.3.3.) were diluted to 1.00 mL and injected in the FIA system. In this case, a linear

400   decrease of the % If with the increase of AR fitted with the equation: $\%If = 85.4\pm0.3 -$

401    $(6.03 \pm 0.09) \times 10^5$ [AR] (M). The difference in the slope observed with respect to that

402   obtained with the calibration graph $(-1.2 (\pm 0.3) \times 10^6 \text{ M}^{-1})$, shows the influence of these

403   matrix in the AR determination. Therefore, the colourant concentration was calculated

404   from the addition standard procedure. An AR amount of 0.30 ± 0.01 mg/g (n=3) was

405   obtained in this sample with a recovery of   96%, evaluated at 2.00×10^{-5} M

406   concentration level.

407   FIGURE 5 HERE

408

409

410

411

3.3.5. HPLC-UV-Vis experiments

In order to validate the result obtained by the FIA-based methodology, both the carbonated drink and the powder for preparation of gelatines were further analysed by HPLC-UV-Vis detection following a procedure previously reported (Yu & Fan, 2016). Figure S8 shows the chromatographs corresponding to increasing AR concentrations. As observed, AR was detected at a retention time (t_R) of 7.6 min and the increase of the signal with AR concentration. Under these conditions, the area values recorded for the injection of the samples, prepared as described before, were $(2.18 \pm 0.01) \times 10^5$ for the carbonated drink and $(1.65 \pm 0.03) \times 10^4$ in the case of the gelatine sample. From the slope of the calibration curve $(1.76 \pm 0.8) \times 10^{10}$ Area/ M), AR concentrations of 61.4 $\pm$ 0.3 mg/L (n=3) and 0.297 ± 0.006 mg/g (n=3) were respectively obtained. These results are in very good agreement with that found with the FIA method proposed allowing us to confirm that the herein reported method works for routine determination of this food additive in real samples.

426

4. Conclusions

In this work, we have demonstrated that dots of MoS_2 results an interesting nanomaterial for the analytical method development based on its fluorescence properties. The HR-TEM reveals very small nanoparticles of 3.4 nm with a hexagonal lattice structure consistent with the (100) diffraction planes. This nanomaterial presents a fluorescence response with a maximum centred at 458 nm when excited with an excitation wavelength of 370 nm. The inhibition of the MoS_2-dots fluorescence signal is

19

434   produced due to the interaction with the dye AR as analyte. The simultaneous injection

435   of the nanomaterial and the analyte in the flow system allows monitoring of the AR

436   concentration. After parameters optimization, the obtained results reveal a sensitive

437   method with a LOD of 1.7×10^{-6} M and a sample frequency of 180 samples/h. This

438   method was applied in the AR determination in a carbonated commercial drink and

439   powder for gelatine with a recovery of 105 % and 96%, respectively. These results were

440   in good agreement with the obtained with a HPLC-UV-Vis method.

441   **5. Acknowledgements**

445

446   **6. References**

447   Al Shamari, Y. M. G., Alwarthan, A. A., Wabaidur, S. M., Khan, M. A., Alqadami, A.

448   A., & Siddiqui, M. R. (2020). New Ultra Performance liquid chromatography-mass

449   spectrometric method for the determination of allura red in soft drinks using

450   corncob as solid phase extraction sorbent: Analysis and food waste management

451   approach. *Journal of King Saud University - Science*, *32*(1), 1135–1141.

452   https://doi.org/10.1016/j.jksus.2019.10.011

453   Bişgin, A. T. (2019). Simultaneous Extraction and Determination of Allura Red (E129)

454   and Brilliant Blue FCF (E133) in Foodstuffs by Column Solid-Phase

455   Spectrophotometry. *Journal of AOAC International*, *102*, 181–188.

456   Bouša, D., Mayorga-Martinez, C. C., Mazánek, V., Sofer, Z., Boušová, K., & Pumera,

457   M. (2018). MoS2 Nanoparticles as Electrocatalytic Labels in Magneto-

Immunoassays. *ACS Applied Materials and Interfaces*, *10*(19), 16861–16866. https://doi.org/10.1021/acsami.8b01607

Cao, H., Huang, Y., Xie, Y., Shi, W., Fu, C., & He, W. (2018). A fast-responsive fluorescent probe for sensitive detection of graphene oxide based on MoS_2 quantum dots. *The Analyst*, *143*(13), 3107–3113. https://doi.org/10.1039/C8AN00849C

Carocho, M., Barreiro, M. F., Morales, P., & Ferreira, I. C. F. R. (2014). Adding Molecules to Food , Pros and Cons : A Review on Synthetic and Natural Food Additives. *Comprehensive Reviews in Food Science and Food Safety*, *13*, 377–399. https://doi.org/10.1111/1541-4337.12065

Coleman, J. N., Lotya, M., O'Neill, A., Bergin, S. D., King, P. J., Khan, U., Young, K., Gaucher, A., De, S., Smith, R. J., Shvets, I. V., Arora, S. K., Stanton, G., Kim, H-Y., Lee, K., Kim, G. T., Duesberg, G. S., Hallam, T., Boland, J. J., Wang, J. J., Donegan, J. F., Grunlan, J. C., Moriarty, G., Shmeliov, A., Nicholls, R. J., Perkins, J. M., Grieveson, E. M., Theuwissen, K., McComb, D. W., Nellist, P. D., Nicolosi, V. (2011). Two-Dimensional Nanosheets Produced by Liquid Exfoliation of Layered Materials. *Science*, *331*(6017), 568–571. https://doi.org/10.1126/science.1194975

Damodaran, S., Parkin, K. L., & Fennema, O. R. (2007). *Food Science and Technology*. Florida:Boca Ratón, (Chapter 1).

Deroco, P. B., Medeiros, R. A., Rocha-filho, R. C., & Fatibello-filho, O. (2018). Selective and simultaneous determination of indigo carmine and allura red in candy samples at the nano-concentration range by fl ow injection analysis with multiple pulse amperometric detection. *Food Chemistry*, *247*(November 2017), 66–72. https://doi.org/10.1016/j.foodchem.2017.12.006

483   Guo, X., Wang, Y., Wu, F., Ni, Y., & Kokot, S. (2015). The use of tungsten disulfide

484   dots as highly selective, fluorescent probes for analysis of nitrofurazone. *Talanta*,

485   *144*, 1036–1043. https://doi.org/10.1016/j.talanta.2015.07.055

486   Ha, H. D., Han, D. J., Choi, J. S., Park, M., & Seo, T. S. (2014). Dual Role of Blue

487   Luminescent MoS_2 Quantum Dots in Fluorescence Resonance Energy Transfer

488   Phenomenon. *Small*, *10*(19), 3858–3862. https://doi.org/10.1002/smll.201400988

489   Huang, X., Zeng, Z., & Zhang, H. (2013). Metal dichalcogenide nanosheets:

490   preparation, properties and applications. *Chemical Society Reviews*, *42*(5), 1934–

491   1946. https://doi.org/10.1039/c2cs35387c

492   Ivani de Andrade, F., Florindo Guedes, M. I., Pinto Vieira, Í. G., PereiraMendes, N. F.,

493   Salmito Rodrigues, P. A., Costa Maia, C. S., Marqués Ávila, M. M., de Matos

494   Ribeiro, L. (2014). Determination of synthetic food dyes in commercial soft drinks

495   by TLC and ion-pair HPLC. *Food Chemistry*, *157*, 193–198.

496   https://doi.org/10.1016/j.foodchem.2014.01.100

497   Lakowicz, J. R. (2006). *Principles of Fluorescence Spectroscopy* .New York, (Chapter

498   8)

499   Lesnyak, V., Gaponik, N., & Eychmu, A. (2013). Colloidal semiconductor nanocrystals:

500   the aqueous approach. *Chemical Society Reviews*, *42*, 2905–2929.

501   https://doi.org/10.1039/c2cs35285k

502   Li, B. L., Wang, J., Zou, H. L., Garaj, S., Lim, C. T., Xie, J., Li, N. B., Leong, D. T.

503   (2016). Low-Dimensional Transition Metal Dichalcogenide Nanostructures Based

504   Sensors. *Advanced Functional Materials*, *26*(39), 7034–7056.

505   https://doi.org/10.1002/adfm.201602136

506   Liu, Q., Hu, C., & Wang, X. (2016). A facile one-step method to produce MoS_2

507   quantum dots as promising bio-imaging materials. *RSC Advances*, *6*(30), 25605–

508   25610. https://doi.org/10.1039/c6ra00572a

509   Liu, X., Zhang, W., Huang, L., Hu, N., Liu, W., Liu, Y., Li, S., Yang, C., Suo, Y.,

510   Wang, J. (2018). Fluorometric determination of dopamine by using molybdenum

511   disulfide quantum dots. *Microchimica Acta*, *185*(4).

512   https://doi.org/10.1007/s00604-018-2771-0

513   Magerusan, L., Pogacean, F., Coros, M., Socaci, C., Pruneanu, S., Leostean, C., & Pana,

514   I. O. (2018). Green methodology for the preparation of chitosan / graphene

515   nanomaterial through electrochemical exfoliation and its applicability in Sunset

516   Yellow detection. *Electrochimica Acta*, *283*, 578–589.

517   https://doi.org/10.1016/j.electacta.2018.06.203

518   Mazdeh, F. Z., Moradi, Z., Moghaddam, G., Moradi-Khatoonabadi, Z., Aftabdari, F. E.,

519   Badaei, P., & Hajimahmoodi, M. (2016). Determination of synthetic food colors,

520   caffeine, sodium benzoate and potassium sorbate in sports drinks. *Tropical Journal*

521   *of Pharmaceutical Research*, *15*(1), 183–188. https://doi.org/10.4314/tjpr.v15i1.25

522   Rodriguez, J. A., Ibarra, I. S., Miranda, J. M., Barrado, E., & Santos, E. M. (2016).

523   Magnetic solid phase extraction based on fullerene and activated carbon adsorbents

524   for determination of azo dyes in water samples by capillary electrophoresis.

525   *Analytical Methods*, *8*(48), 8466–8473. https://doi.org/10.1039/c6ay02631a

526   Shen, Y., Zhang, X., Prinyawiwatkul, W., & Xu, Z. (2014). Simultaneous determination

527   of red and yellow artificial food colourants and carotenoid pigments in food

528   products. *Food Chemistry*, *157*, 553–558.

529   https://doi.org/10.1016/j.foodchem.2014.02.039

530   Silva, M. L. S., Garcia, M. B. Q., Lima, J. L. F. C., & Barrado, E. (2007). Voltammetric

531   determination of food colorants using a polyallylamine modified tubular electrode

532   in a multicommutated flow system. *Talanta*, *72*(1), 282–288.

https://doi.org/10.1016/j.talanta.2006.10.032

Sinha, A., Dhanjai, Tan, B., Huang, Y., Zhao, H., Dang, X., Chen, J., Jain, R. (2018). MoS_2 nanostructures for electrochemical sensing of multidisciplinary targets: A review. *TrAC - Trends in Analytical Chemistry*, *102*, 75–90. https://doi.org/10.1016/j.trac.2018.01.008

Štengl, V., & Henych, J. (2013). Strongly luminescent monolayered MoS_2 prepared by effective ultrasound exfoliation. *Nanoscale*, *5*, 3387–3394. https://doi.org/10.1039/c3nr00192j

Sun, J., Li, X., Guo, W., Zhao, M., Fan, X., Dong, Y., Xu, C., Deng, J., Fu, Y. (2017). Synthesis Methods of Two-Dimensional MoS_2: A Brief Review. *Crystals*, *7*(7), 198. https://doi.org/10.3390/cryst7070198

Tang, Y., Sun, Z., Shen, J., Yu, J., Wang, S., Hao, J., Wang, B., Huang, Y., Liu, X., Zhuang, H. (2018). Peptide modified gold nanoclusters as a novel fluorescence detector based on quenching system of detecting Allura red. *Analytical Methods*, *10*, 5672–5678. https://doi.org/10.1039/c8ay01494a

Trojanowicz, M., & Kołacińska, K. (2016). Recent advances in flow injection analysis. *The Analyst*, *141*(7), 2085–2139. https://doi.org/10.1039/C5AN02522B

Union, C. of the E. (1994). European Parliament and Council Directive 94/35/EC of 30 June 1994 of sweeteners for use in foodstuffs. https://op.europa.eu/en/publication-detail/-/publication/576c6110-0270-429a-b445-8bdb40025cb4/language-en.

Vidal, M., Garcia-Arrona, R., Bordagaray, A., Ostra, M., & Albizu, G. (2018). Simultaneous determination of color additives tartrazine and allura red in food products by digital image analysis. *Talanta*, *184*(December 2017), 58–64. https://doi.org/10.1016/j.talanta.2018.02.111

Vilian, A. T. E., Dinesh, B., Kang, S. M., Krishnan, U. M., Huh, Y. S., & Han, Y. K.

(2019). Recent advances in molybdenum disulfide-based electrode materials for electroanalytical applications. *Microchimica Acta*, *186*, 203. https://doi.org/10.1007/s00604-019-3287-y

Wang, Yichao, Ou, J. Z., Balendhran, S., Chrimes, A. F., Mortazavi, M., Yao, D. D., Field, M. R., Latham, K., Bansal, V., Friend, J.R., Zhuiykov, S., Medhekar, N. V., Strano, M. S., Kalantar-Zadeh, K. (2013). Electrochemical control of photoluminescence in two-dimensional MoS_2 nanoflakes. *ACS Nano*, *7*(11), 10083–10093. https://doi.org/10.1021/nn4041987

Wang, Yong, & Ni, Y. (2014). Molybdenum disulfide quantum dots as a photoluminescence sensing platform for 2,4,6-trinitrophenol detection. *Analytical Chemistry*, *86*(15), 7463–7470. https://doi.org/10.1021/ac5012014

Wang, Z., & Dai, Z. (2015). Carbon nanomaterial-based electrochemical biosensors: An overview. *Nanoscale*, *7*(15), 6420–6431. https://doi.org/10.1039/c5nr00585j

Wilcoxon, J. P., Newcomer, P. P., & Samara, G. A. (1997). Synthesis and optical properties of MoS2 and isomorphous nanoclusters in the quantum confinement regime. *Journal of Applied Physics*, *81*(12), 7934–7944. https://doi.org/10.1063/1.365367

Xu, H., Yang, X., Li, G., Zhao, C., & Liao, X. (2015). Green Synthesis of Fluorescent Carbon Dots for Selective Detection of Tartrazine in Food Samples. *Journal of Agricultural and Food Chemistry*, *63*(30), 6707–6714. https://doi.org/10.1021/acs.jafc.5b02319

Xu, S., Li, D., & Wu, P. (2015a). One-pot, facile, and versatile synthesis of monolayer MoS2 /WS2 quantum dots as bioimaging probes and efficient electrocatalysts for hydrogen evolution reaction. *Advanced Functional Materials*, *25*(7), 1127–1136. https://doi.org/10.1002/adfm.201403863

583   Yu, Y., & Fan, Z. (2016). Magnetic solid-phase extraction coupled with HPLC for the

584   determination of Allura Red in food and beverage samples. *Food Additives and*

585   *Contaminants - Part A*, *33*(10), 1527–1534.

586   https://doi.org/10.1080/19440049.2016.1231937

587   Zhang, W., Wang, Y., Zhang, D., Yu, S., Zhu, W., Wang, J., … Wang, J. (2015). A

588   one-step approach to the large-scale synthesis of functionalized MoS_2 nanosheets

589   by ionic liquid assisted grinding. *Nanoscale*, *7*(22), 10210–10217.

590   https://doi.org/10.1039/c5nr02253c

591   Zhang, X., Lai, Z., Liu, Z., Tan, C., Huang, Y., & Li, B. (2015). A Facile and Universal

592   Top-Down Method for Preparation of Monodisperse Transition-Metal

593   Dichalcogenide Nanodots. *Angewandte Chemie*, *54*, 5425–5428.

594   https://doi.org/10.1002/anie.201501071

595   Zhao, M., Chen, A.-Y., Huang, D., Chai, Y.-Q., Zhuo, Y., & Yuan, R. (2017). MoS_2

596   Quantum Dots as New Electrochemiluminescence Emitters for Ultrasensitive

597   Bioanalysis of Lipopolysaccharide. *Analytical Chemistry*, *89*(16), 8335–8342.

598   https://doi.org/10.1021/acs.analchem.7b01558

599
600

Figure Captions

Figure 1. (A) HR-TEM image of the MoS_2-dots with 10 nm scale. The inset shows a selected area electron diffraction (SAED) pattern. (B) Higher magnification showing the lattice fringes of a MoS_2-dots. (C) A line profile indicating the d-spacing in the selected MoS_2-dots.

Figure 2. (A) Absorption spectra of AR (a) and fluorescence spectra of MoS_2-dots at different λ_{exc} (dotted lines). (B) Fluorescence spectra of MoS_2-dots in absence (a) and in presence of 2.0×10^{-5} M AR (b). $\lambda_{exc} = 370$ nm. MoS_2-dots diluted 1:100 in H_3PO_4/NaH_2PO_4 0.1M pH 2.

Figure 3. Fluorescence inhibition at 475 nm for increasing AR concentrations at different temperatures. The legend includes the Ksv values calculated from the slopes of the corresponding experiments.

Figure 4. A) FIAgrams of MoS_2-dots and MoS_2-dots with increasing concentrations of AR. B) Calibration plot of %If_0 with increasing concentration of AR. L= 40 cm; Di = 0.5 mm; Q = 3 mL/min; V_{inj} = 100 μL. MoS_2-dots 1:150 in H_3PO_4/NaH_2PO_4 0.1M pH 2. $\lambda_{exc} = 370$ nm; $\lambda_{em} = 475$ nm.

Figure 5. FIAgrams of MoS_2-dots and MoS_2-dots with non-spiked and spiked samples L= 40 cm; Di = 0.5 mm; Q = 3 mL/min; V_{inj} = 100 μL. MoS_2-dots 1:150 in H_3PO_4/NaH_2PO_4 0.1M pH 2. $\lambda_{exc} = 370$ nm; $\lambda_{em} = 475$ nm.
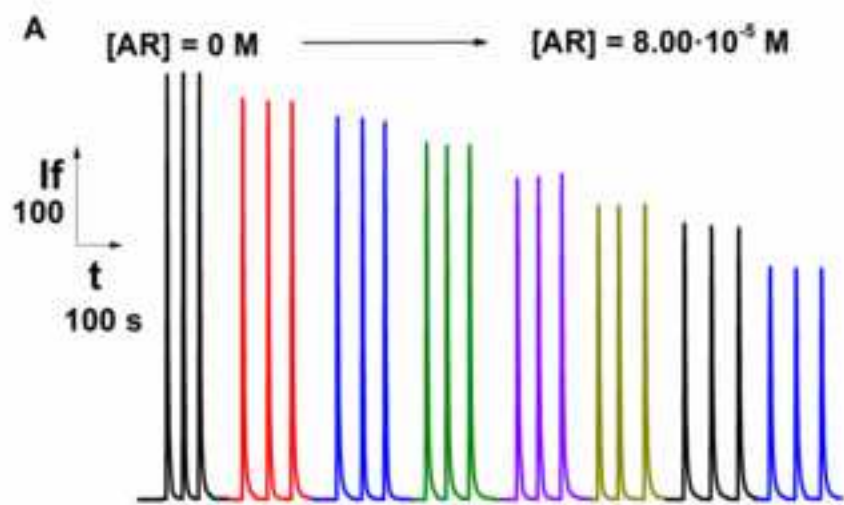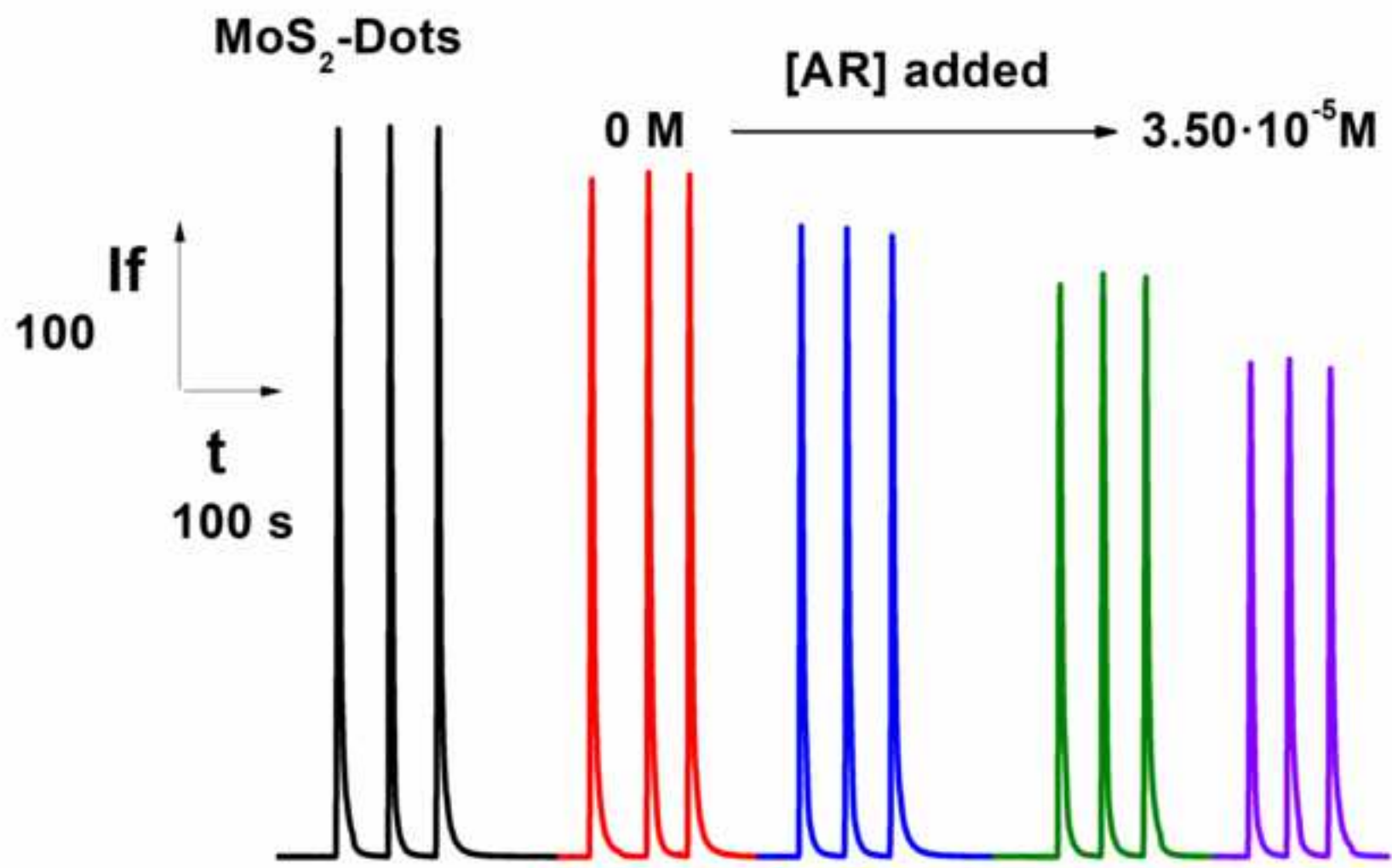
A) B) C)
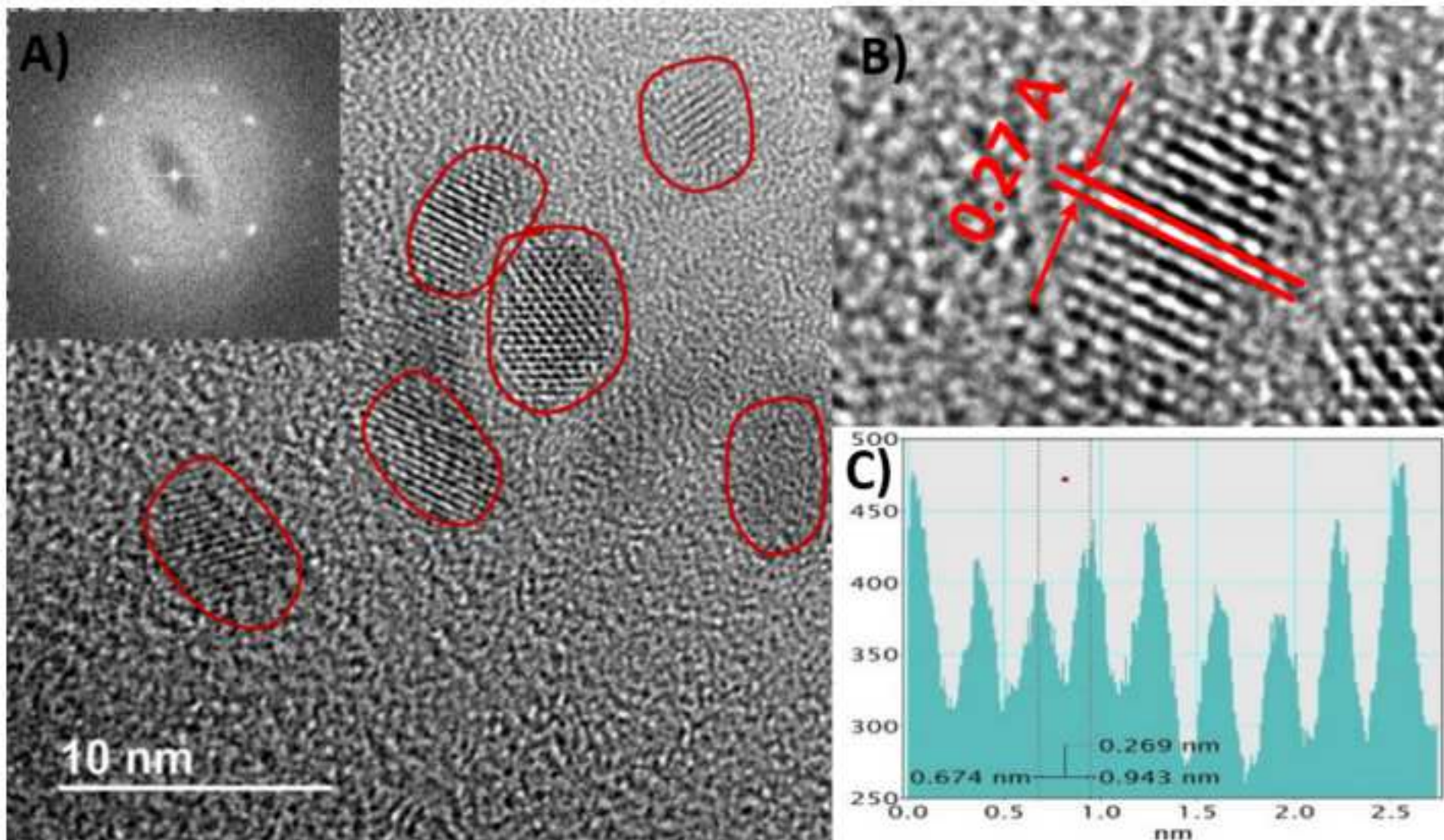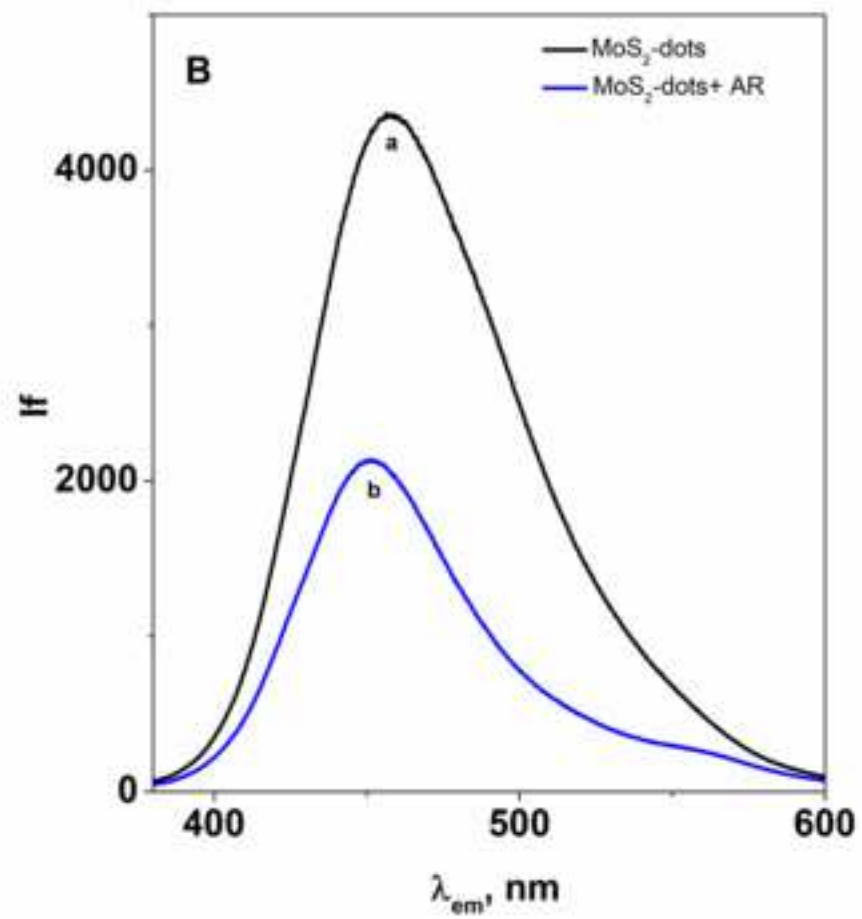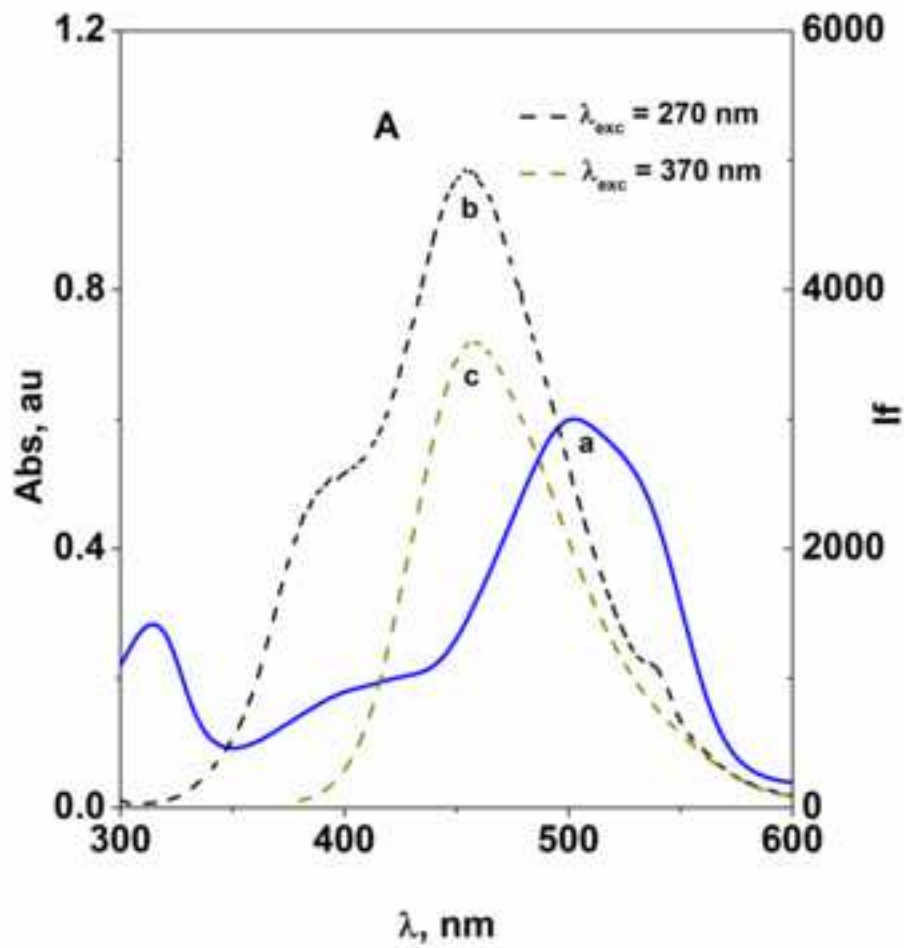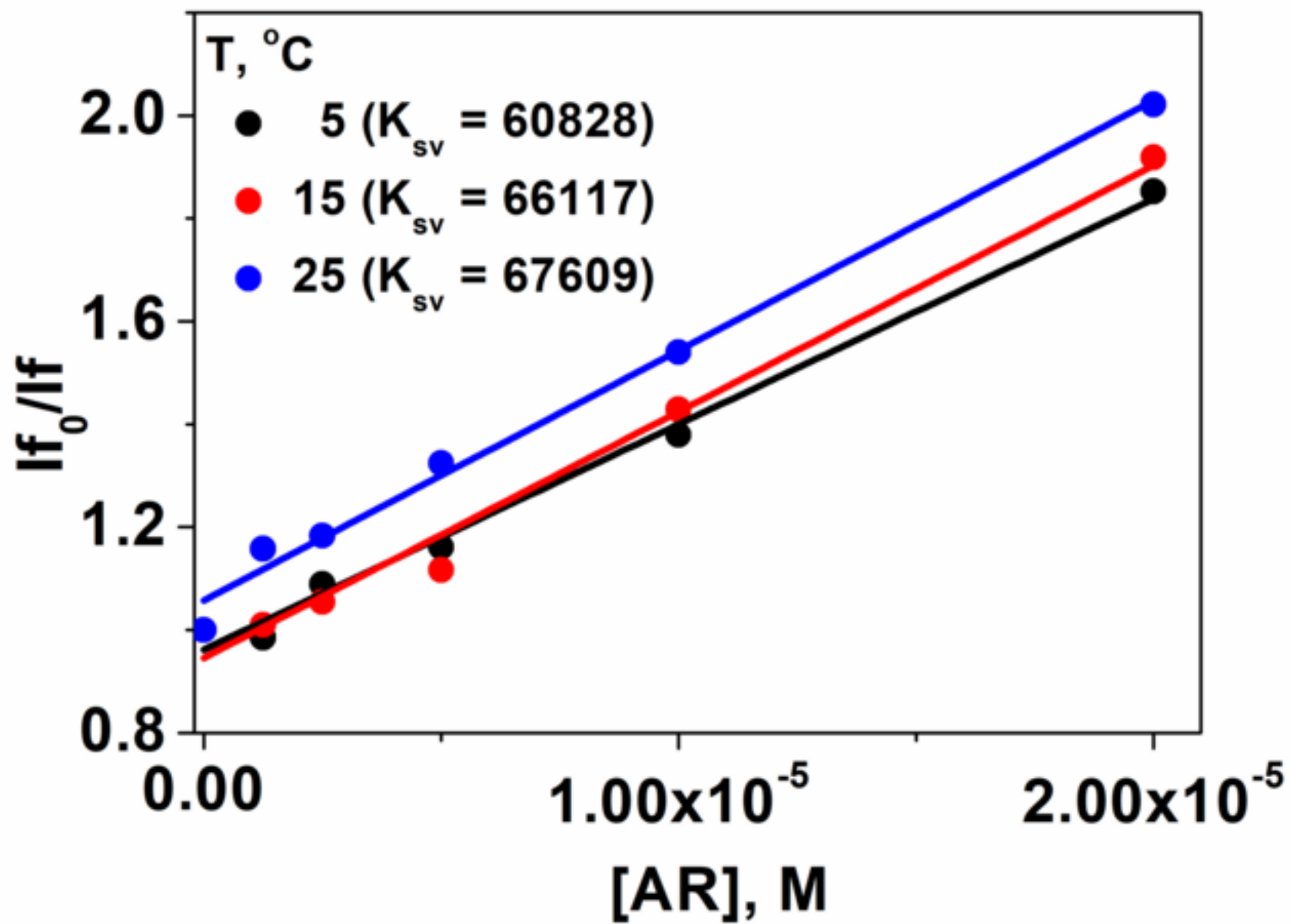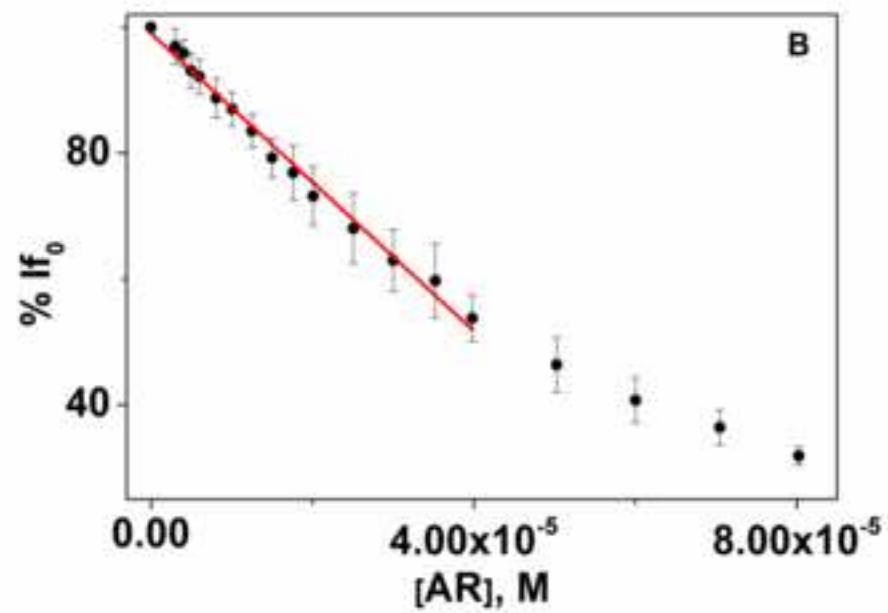
Supplementary Material

MoS$_2$ quantum dots for on-line fluorescence determination of the food additive allura red in beverage.

Alicia Coloma[a], María del Pozo[a]*, Rut Martínez-Moro[a], Elias Blanco[a], Pedro Atienzar[b], Lorenzo Sánchez[c], María Dolores Petit-Domínguez[a], Elena Casero[a], Carmen Quintana[a]

[a]*Departamento de Química Analítica y Análisis Instrumental, Universidad Autónoma de Madrid, Cantoblanco, 28049 Madrid, Spain.*

[b]*Instituto Universitario de Tecnología Química CSIC-UPV, Departamento de Química, Universidad Politécnica de Valencia, 46022 Valencia, Spain.*

[c] *Departamento de Medio Ambiente. Geología Ambiental Aplicada. CIEMAT. Avda. Complutense, 40 Edif. 85, 28040 Madrid. Spain*

*maria.delpozo@uam.es; Phone: +34 914975619; Fax: +34914974931
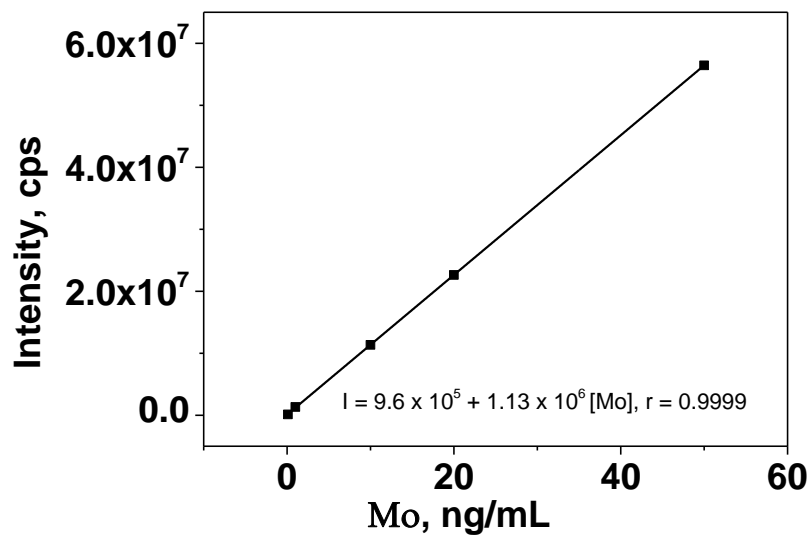
Figure S1. ICP-MS calibration graphs corresponding to Mo determination in the
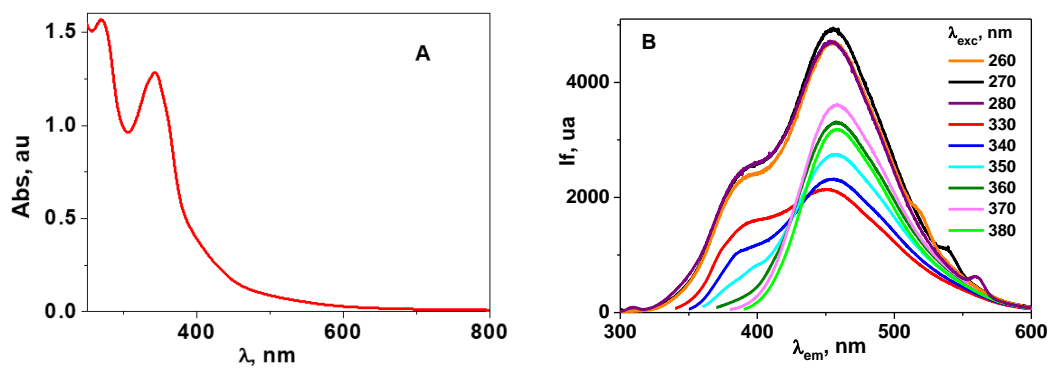
synthetized suspensions

Figure S2. A: UV-VIS absorption spectrum of MoS_2-dots 1:100 diluted in water. B:

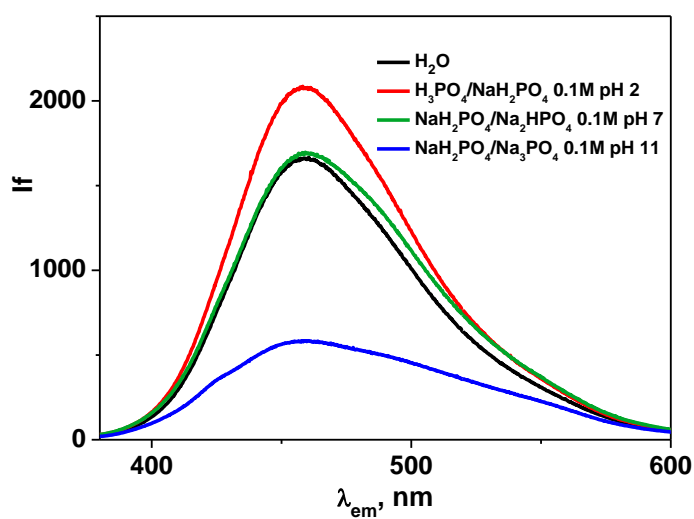MoS_2-dots fluorescence spectra recorded at λ_{exc} between 260-380 nm.

Figure S3. MoS$_2$-dots spectra recorded for 1:100 dilution at different pH values. λ_{exc} = 370 nm.
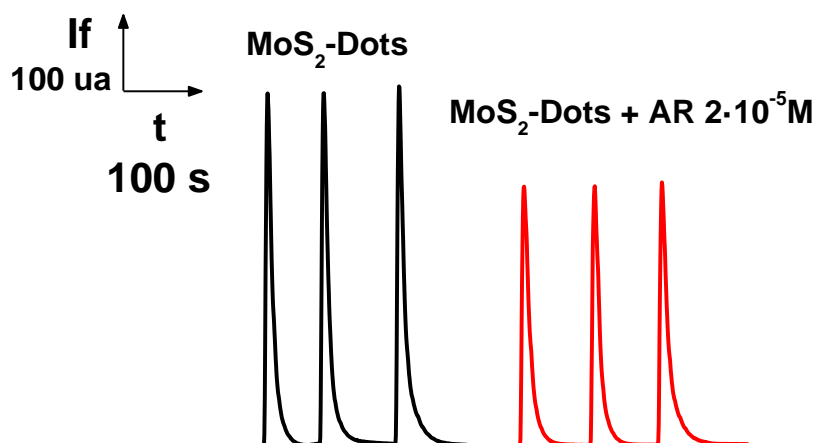

Figure S4. FIA-graphs of MoS$_2$-dots and MoS$_2$-dots-AR. [AR] = 2.0×10^{-5} M; H$_3$PO$_4$/NaH$_2$PO$_4$ 0.1 M pH2; MoS$_2$-dots diluted 1:150 in H$_3$PO$_4$/NaH$_2$PO$_4$ 0.1 M pH 2. Reactor length (L) = 40 cm; Reactor internal diameter (Di) = 0.5 cm; Injection volume (V$_{inj}$) = 100 μL; Caudal (Q) = 1 mL/min; λ_{exc} = 370 nm; λ_{em} = 475 nm.
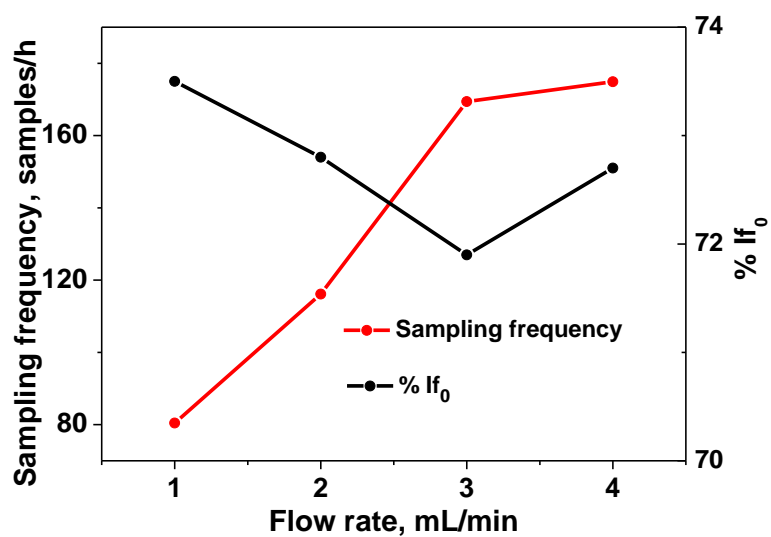
Figure S5. % If_0 and sampling frequency variation with the carrier flow rate. L = 40 cm; Di = 0.5 cm; V_{iny} = 100 μL. MoS_2-dots 1:150 in H_3PO_4/NaH_2PO_4 0.1M pH 2. [AR] = $2.00 \cdot 10^{-5}$ M, λ_{exc} = 370 nm; λ_{em} = 475 nm.
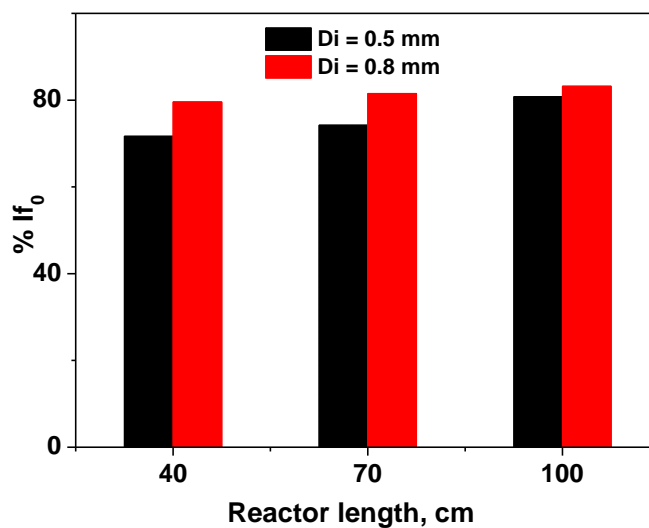

Figure S6. Influence of both, length and internal diameter of the reactor, in the % If_0. V_{iny} = 100 μL; Q = 3 mL/min. MoS_2-dots 1:150 in 0.1M H_3PO_4/NaH_2PO_4 pH 2. [AR] = $2.00 \cdot 10^{-5}$ M, λ_{exc} = 370 nm; λ_{em} = 475 nm.
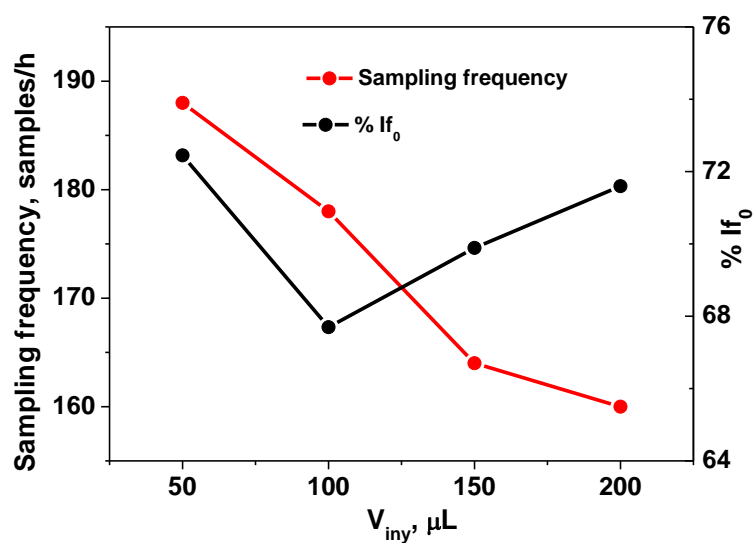
Figure S7. Variation of both, % If_0 and sampling frequency, with the injection volume. L= 40 cm; Di = 0.5 mm; Q = 3 mL/min. MoS_2-dots 1:150 in H_3PO_4/NaH_2PO_4 0.1M pH 2. [AR] = 2.00·10^{-5} M, λ_{exc} = 370 nm; λ_{em} = 475 nm.
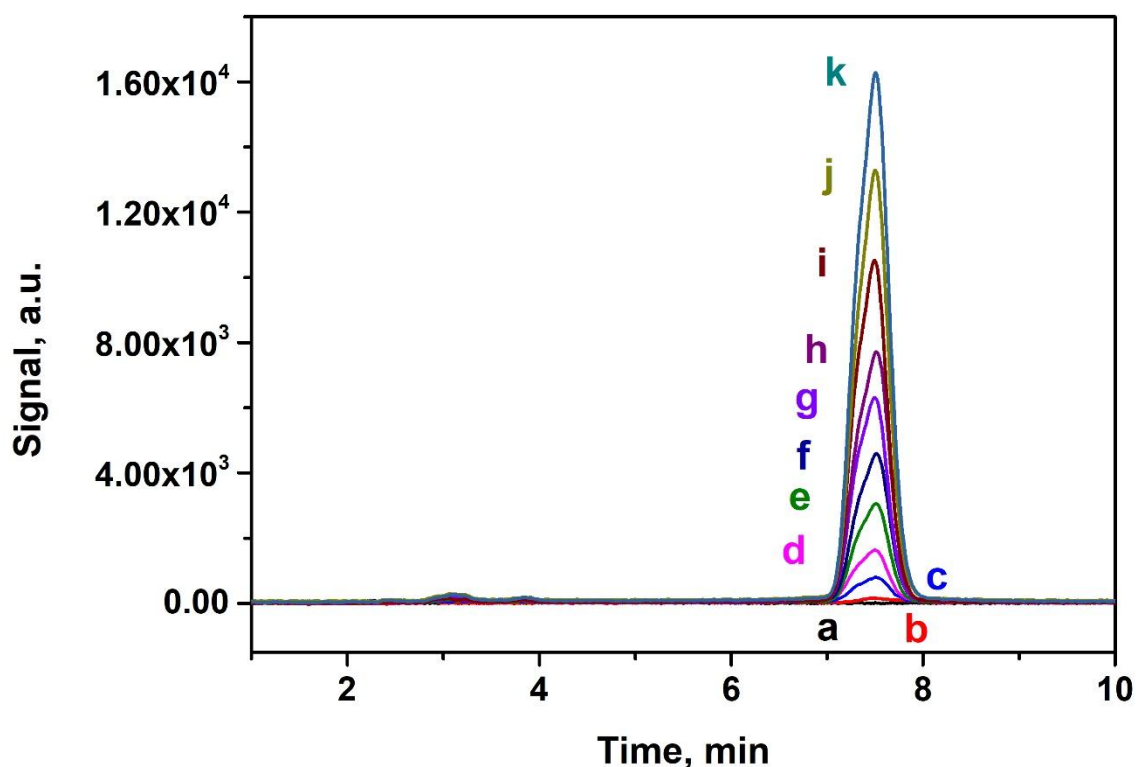

Figure S8. Chromatograms corresponding to solutions containing increasing concentrations of AR recorded at the HPLC-UV-Vis system (a) Mobile phase, (b) 2.0 10^{-7}, (c) 1.1 10^{-6},(d) 2.1 10^{-6},(e) 4.0 10^{-6}, (f) 6.0 10^{-6}, (g) 8.1 10^{-6}, (h) 1.0 10^{-5}, (i) 1.3 10^{-5} M, (j) 1.6 10^{-5} M and (k) 2.0 10^{-5} M.

Table S1. Hydrodynamic and geometrical parameter optimization.

Parameter	Range assays	Optimal value
[MoS$_2$-Dots] (dilution 1:X)	50-200	150
Flow rate (Q) (mL/min)	1-4	3
Reactor length (L) (cm)	40-100	40
Reactor internal diameter (Di) (mm)	0.5-0.8	0.5
Injection volume (V$_{inj}$) (μL)	50-200	100

Table S2. Comparative methods for AR determination

Method	LOD (mol/L)	Linear Range (mol/L)	Reference
Digital image analysis	1.29×10^{-6}	$4.29 \times 10^{-6} - 5.57 \times 10^{-5}$	(Vidal, Garcia-Arrona, Bordagaray, Ostra, & Albizu, 2018)
Amperometric-FIA (polyallylamine - GCTE)	1.40×10^{-6}	$1.00 \times 10^{-5} - 1.50 \times 10^{-4}$	(Silva, Garcia, Lima, & Barrado, 2007)
MPA-FIA (BDD/p-silicon)	7.00×10^{-9}	$4.00 \times 10^{-8} - 7.70 \times 10^{-7}$	(Deroco, Medeiros, Rocha-filho, & Fatibello-filho, 2018)
MSPE-CE	4.29×10^{-6}	$1.29 \times 10^{-5} - 8.58 \times 10^{-5}$	(Rodriguez, Ibarra, Miranda, Barrado, & Santos, 2016)
AuNCs-Peptide Fluorescence	6.67×10^{-7}	$2.00 \times 10^{-6} - 9.00 \times 10^{-5}$	(Tang et al., 2018)
UPLC-MS	2.57×10^{-8}	$1.00 \times 10^{-7} - 2.79 \times 10^{-6}$	(Al Shamari et al., 2020)
HPLC-UV	1.09×10^{-6}	-	(Mazdeh et al., 2016)
MoS_2-dots FIA-fluorescence	1.70×10^{-6}	$5.00 \times 10^{-6} - 4.00 \times 10^{-5}$	This work

GCTE: Glassy carbon tubular electrode; MPA-FIA: Multiple pulse amperometric Flow injection analysis. BDD/p-silicon: Boron-doped diamond/ p-silicon; MSPE-CE: Magnetic solid phase extraction coupled to capillary electrophoresis; AnNCs-Peptide: gold nanoclusters modified with peptide; UPLC-MS: Ultra performance liquid chromatography-mass spectrometry; HPLC-UV: High performance liquid chromatography couple to ultraviolet detector